ELSEVIER

A New Approach for Remote Sensing of Canopy-Absorbed Photosynthetically Active Radiation. I: Total Surface Absorption

Zhanqing Li[*] *and Louis Moreau*[†]

The canopy-absorbed photosynthetically active radiation $APAR_{CAN}$ is the solar energy consumed in the canopy photosynthetic process. Due to the difficulty of acquiring extensive ground-based observations, increasing efforts are being devoted to estimate $APAR_{CAN}$ from optical satellite measurements. So far, $APAR_{CAN}$ has been obtained from the downwelling PAR at the surface (SFC), $PAR_{SFC}\downarrow$, and the fraction of PAR absorbed by a canopy, FPAR. This study proposes a new approach which defines $APAR_{CAN}$ as the product of $APAR_{SFC}$ and RPAR. $APAR_{SFC}$ is the total PAR absorbed by all surface materials including canopy, soil, litter, etc., while RPAR is the ratio of the PAR absorbed by the green canopy only, to $APAR_{SFC}$. The advantage of this approach is that $APAR_{SFC}$ can be determined more accurately and readily than $PAR_{SFC}\downarrow$, while the determination of RPAR is as accurate as that of FPAR with the same difficulties. The whole approach is introduced in two parts. Part I, as presented in this article, deals with the retrieval of $APAR_{SFC}$. Using a complex atmospheric radiative transfer model, $APAR_{SFC}$ is related to the upwelling PAR reflected at the top of the atmosphere (TOA), $PAR_{TOA}\uparrow$. The relationship is independent of cloud parameters and surface conditions, and moderately dependent on ozone amount and aerosol optical properties. A parameterization was developed to estimate $APAR_{SFC}$ from $PAR_{TOA}\uparrow$, which is inferred from satellite measurements in the visible bands. Error analyses were made using data from both model simulations and field observations. The parameterization is valid to within 5 W m^{-2} compared to the results of detailed radiation model simulations. A preliminary comparison against FIFE ground observations showed a bias error of -2.7 W m^{-2} and a standard error of 21.9 W m^{-2} for the instantaneous estimates of $APAR_{SFC}$.

INTRODUCTION

Photosynthetically active radiation (PAR), is the solar radiation in the wavelength interval between approximately 400–700 nm (i.e., 0.4–0.7 μm). The PAR absorbed by green canopy, $APAR_{CAN}$, is directly linked to photosynthesis, net primary productivity (NPP), and the carbon cycle (Monteith, 1971; Budyko, 1980). Since PAR accounts for nearly half of the total solar radiation at the surface, it also contributes significantly to the exchanges of energy and water between the surface and the atmosphere of the Earth. Therefore, knowledge of the geographical distribution and temporal variation in $APAR_{CAN}$ is necessary for modeling the dynamics of the Earth's ecosystem and climate system (Sellers et al., 1986; Trenberth, 1992).

So far, $APAR_{CAN}$ has been derived from the downwelling PAR reaching the surface, $PAR_{SFC}\downarrow$, and the fraction of $PAR_{SFC}\downarrow$ intercepted by the canopy, FPAR. Unfortunately, there are very limited surface observations of both $PAR_{SFC}\downarrow$ and FPAR. Most PAR observations were made in field experiments of short durations for research purposes (e.g., Demetriades-Shah et al., 1992; Pinter, 1993). As a result, $PAR_{SFC}\downarrow$ data are often obtained by converting shortwave (SW) insolation measurements (0.285–3.0 μm) made by pyranometers in radiation network (Rao, 1984; Eck and Dye, 1991). This may introduce appreciable errors as the conversion factor is not a constant but ranges from 0.4 to 0.6 depending on atmospheric and cloud conditions, solar zenith angle (SZA), and aerosol optical properties (Baker and Frouin, 1987; Pinker and Laszlo, 1992a). Furthermore, the num-

[*]Canada Centre for Remote Sensing, Ottawa, Ontario
[†]Intera Information Technologies Ltd., Ottawa, Ontario

Address correspondence to Zhanqing Li, Canada Centre for Remote Sensing, 588 Booth, Ottawa, Ontario, Canada, K1A 0Y7.
Received 19 August 1994; revised 7 April 1995.

REMOTE SENS. ENVIRON. 55:175–191 (1996)
©Government of Canada, 1996
Published by Elsevier Science, Inc.

0034-4257 / 96 / $15.00
SSDI 0034-4257(95)00097-K

ber of pyranometers deployed in the global radiation network is too small to accurately map the geographical distribution of SW insolation (Li et al., 1995) and $PAR_{SFC}\downarrow$. Acquiring FPAR is more challenging, as it entails the measurements of net PAR fluxes at the top and bottom of the canopy. As a result, there have been even less observations for FPAR than for $PAR_{SFC}\downarrow$.

The ability to retrieve the SW surface radiation budget (SRB) from satellite (Schmetz, 1989; Pinker et al., 1995) suggests that $PAR_{SFC}\downarrow$ and $APAR_{CAN}$ may be inferred from satellites that offer global coverage at moderate and high spatial resolutions. Since $PAR_{SFC}\downarrow$ differs from SW insolation only in the spectral range, the methodology developed for the retrieval of SW insolation should be, in principle, applicable to the retrieval of $PAR_{SFC}\downarrow$. In fact, the majority of the $PAR_{SFC}\downarrow$ techniques that have been proposed are similar, in concept, to those developed for retrieving surface SW insolation (Frouin and Pinker, 1995). For example, the Frouin and Gautier (1990) method was based on the framework of Gautier et al. (1980) designed for retrieving SW insolation with the following modifications for retrieving $PAR_{SFC}\downarrow$. Cloud absorption was set to zero, considering that clouds have negligible absorption across the PAR wavelengths. Cloud reflection was determined by comparing clear-sky and cloudy-sky satellite measurements and solving a quadratic equation containing parameters regarding the radiative properties of the atmosphere, cloud, and surface. The clear-sky model coefficients were modified to distinguish $PAR_{SFC}\downarrow$ from SW insolation. Likewise, the same methodology used in the retrieval of surface insolation (Pinker and Laszlo, 1992b) was followed by Pinker and Laszlo (1992a) to derive $PAR_{SFC}\downarrow$, the only difference being the integration interval. Their method includes three basic steps. First, relationships were established between atmospheric transmissivity and the reflectivity at the top of the atmosphere (TOA) under various conditions pertaining to surface, atmosphere, and clouds, on the basis of radiative transfer simulations. Second, the parameters characterizing these conditions were inferred by comparing the model-computed TOA reflectivities with satellite-measured ones. Third, $PAR_{SFC}\downarrow$ was obtained by integrating the downwelling spectral irradiance over the PAR spectrum that were computed using the inferred parameters. The method of Eck and Dye (1991) is an exception in that it was designed specifically to retrieve $PAR_{SFC}\downarrow$. Their method employed the ultraviolet reflectance data from the Total Ozone Mapping Spectrometer (TOMS) instead of visible reflectance data in order to increase the contrast between clouds and the surface and thus improve the estimation of cloud reflectance. $PAR_{SFC}\downarrow$ was then calculated by multiplying a cloud correction factor composed of cloud reflectance with the potential clear-sky PAR insolation that was computed from a parameterization accounting for the effects of the SZA, ozone absorption, Rayleigh scattering, and aerosol absorbing and scattering. Reasonable agreements were found between observed and estimated $PAR_{SFC}\downarrow$ (Frouin and Gautier, 1990; Eck and Dye, 1991; Goward et al., 1994).

In view of the difficulty obtaining FPAR from ground-based observations, attempts have also been made to infer FPAR from satellite observations. FPAR was found to correlate with vegetation indices (VI) (Asrar, 1984; Sellers, 1987; Myneni et al., 1992), which can be derived from satellite visible and near-infrared measurements such as the Advanced Very High Resolution Radiometer (AVHRR) (Tarpley et al., 1984; Los et al., 1994). Using such a relationship, Sellers et al. (1994) derived global monthly fields of FPAR from the global NDVI data set of Los et al. (1994). Dye and Goward (1993) generated a global image of $APAR_{CAN}$ from AVHRR observations using the PAR model of Eck and Dye (1991) and the FPAR formula of Goward and Huemmrich (1992).

We propose an alternative approach to estimate $APAR_{CAN}$ from satellite data, which is described in two parts. Part I, as presented in this article, establishes a relationship between the upwelling PAR reflected at the TOA, $PAR_{TOA}\uparrow$, and the total amount of PAR absorbed by all surface materials below the top of the canopy, $APAR_{SFC}$, using an atmospheric radiative transfer model. Part II, presented in Moreau and Li (1996), concerns with the ratio of the PAR absorbed by green canopy only to $APAR_{SFC}$, RPAR, using a canopy radiative transfer model. The advantages of this approach to the traditional one are explained conceptually in the following section.

CONCEPTS OF THE NEW APPROACH

Figure 1 is a schematic diagram showing PAR transfer from the TOA to the surface. Before PAR photons reached the surface, they undergo absorption by ozone, Rayleigh scattering by atmospheric molecules, Mie scattering by cloud droplets, absorption and scattering by aerosols, etc. Some of the photons reaching the surface will be absorbed by green canopy denoted by $APAR_{CAN}$. The traditional and new methods for determining $APAR_{CAN}$ are expressed by Eqs. (1) and (2), respectively,

$$APAR_{CAN} = PAR_{SFC}\downarrow FPAR, \quad (1)$$

$$APAR_{CAN} = APAR_{SFC}\, RPAR. \quad (2)$$

$APAR_{SFC}$ is expected to be retrieved more accurately and readily than $PAR_{SFC}\downarrow$, as is demonstrated in this article, while estimation of RPAR is as accurate and easy as that of FPAR, which is addressed in the companion paper by Moreau and Li (1996).

It follows from Figure 1 that estimation of $PAR_{SFC}\downarrow$ requires information on transmissivity represented by t_1, t_2, t_3, and cloud amount. The values of t_1, t_2, and t_3

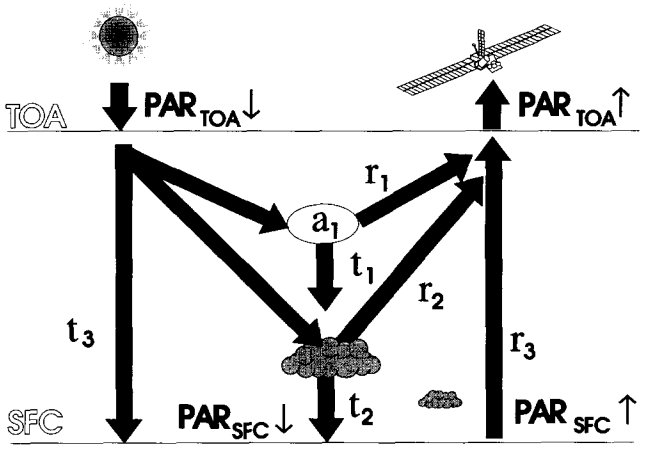

Figure 1. Schematic PAR transfer in the atmosphere. r_1, r_2, and r_3 represent reflection by the atmospheric molecules, cloud droplets, and surface, respectively. t_1 and t_2 denote the transmission of PAR above and below the top of cloud for cloudy atmosphere, respectively, while t_3 is the transmission for clear atmosphere. a_1 denotes PAR absorption by the atmosphere.

cannot be determined unless $PAR_{TOA}\uparrow$ can be decomposed in terms of molecular scattering (r_1), cloud reflection (r_2), and surface reflection (r_3). This in turn requires *a priori* knowledge of the atmosphere, cloud, and surface. Since $PAR_{SFC}\downarrow$ is most sensitive to cloud, retrieval of cloud parameters largely governs the accuracy of the derived $PAR_{SFC}\downarrow$. Hence, the retrieval of reliable cloud information is essential to PAR estimation. Unfortunately, remote sensing of cloud properties is still error-prone, and so is the estimation of $PAR_{SFC}\downarrow$. In comparison, $APAR_{SFC}$ is determined by

$$APAR_{SFC} = PAR_{TOA}\downarrow - PAR_{TOA}\uparrow - APAR_{ATM}, \quad (3)$$

where $PAR_{TOA}\downarrow$ denotes the PAR incident at the TOA which can be computed theoretically. $PAR_{TOA}\uparrow$ can be obtained from satellite visible measurements with spectral and angular corrections. Only the PAR absorbed in the atmospheric column, $APAR_{ATM}$, is unknown. Since clouds do not absorb solar radiation over the PAR spectrum, $APAR_{ATM}$ is much less variable than $PAR_{TOA}\uparrow$. $APAR_{ATM}$ is modified only moderately by atmospheric conditions, in particular, the amounts of ozone and absorbing aerosols. Clouds have a small impact on $APAR_{ATM}$ by backscattering a larger amount of PAR available for absorption in the ozone layer aloft. The ensuing increase in $APAR_{ATM}$ can be accounted for by $PAR_{TOA}\uparrow$, as the two variables are coupled. Therefore, variation in $APAR_{SFC}$ is driven primarily by $PAR_{TOA}\uparrow$. Since no information on clouds is required, $APAR_{SFC}$ should be estimated more accurately and easily than $PAR_{SFC}\downarrow$.

The same philosophy was embodied by Li et al. (1993a) in an attempt to derive SW surface radiation budget (SRB) that is generally based on surface insolation and albedo. Instead of using complex techniques for retrieving the two quantities, a simple algorithm was designed to retrieve SW SRB, as a single variable, from the TOA upwelling flux (Li et al., 1993a). Using their method, a global climatology of SW SRB was readily developed from the Earth Radiation Budget Experiment (ERBE) satellite data (Li and Leighton, 1993). The estimates have no bias errors and small random errors with reference to surface measurements (Li et al., 1993b; 1995). The new approach has been proven to be more accurate, is easier to implement, and requires less input data and computing resources than the traditional one (Li, 1995). Of course, the method for retrieving SW SRB is not valid for retrieving $APAR_{SFC}$ due to the difference in spectral coverage which yields considerable discrepancies between the radiative processes in the two bands. However, the principles are the same, and thus the success with the retrieval of SW radiation lends us some confidence. In fact, the approach should be more successful with PAR than with SW SRB, since clouds have moderate absorption in the near-infrared region, and the bandpasses of space-borne visible sensors are very close to the PAR spectrum.

RELATING $APAR_{SFC}$ TO $PAR_{TOA}\uparrow$

Atmospheric Radiative Transfer Model

Since the objective of this article is to establish a relationship between $APAR_{SFC}$ and $PAR_{TOA}\uparrow$, an atmospheric radiative transfer model suffices. The study is based on an improved version of the radiative transfer model employed in Li et al. (1993a) to simulate various PAR components under a variety of conditions pertaining to the atmosphere, cloud, and surface. It is a doubling-adding model applied to a plane-parallel vertically inhomogeneous atmosphere–surface system (Masuda et al., 1995). The atmosphere is divided into eight homogeneous layers (0–1 km, 1–2 km, 2–4 km, 4–6 km, 6–9 km, 9–13 km, 13–25 km, and 25–100 km). The model accounts for the radiative effects of air molecules, clouds, water vapor, ozone, and aerosol particles. Ozone is contained in the highest model layer; clouds may be placed in any layer; the bulk of aerosol and water vapor is contained in the boundary layers below 2 km. Optical thickness for absorption by ozone, oxygen, and carbon dioxide, and for molecular scattering were obtained from Braslau and Dave (1973) and transmittances were calculated by LOWTRAN 7. Major absorption bands of the atmospheric constituents in the PAR spectral region include the ozone Chappuis band at 0.5 μm and oxygen band at 0.7 μm. Different types of clouds and aerosols were used including stratus cloud (St), cumulus cloud (Cu), stratocumulus cloud (Sc), nimbus cloud (Nb), continental and maritime aerosols of varying optical thicknesses. The optical properties of cloud droplets were

taken from a tabulation given by Stephens (1979), and those for aerosols were given in WCP-112 (1986). The clouds are assumed to be plane-parallel and the cloud droplet phase functions are approximated by the Henyey–Greenstein function. Considering that the reflectivities of most surfaces do not change significantly with wavelength in the PAR spectrum, surface albedos independent of wavelength were assumed. The code has been tested by comparing with another doubling-adding model with a line-by-line scheme. The agreements are very good (Masuda et al., 1995).

The TOA solar spectral data compiled by Iqbal (1983) were adopted. While the model spans the total solar spectrum, this study is limited to the PAR wavelength from 400 nm to 700 nm. The spectral resolution of the model is 5 nm from 400 nm to 610 nm, and 10 nm for wavelengths up to 700 nm. Thus, the total number of spectral intervals for PAR is 51. For each atmosphere–surface combination, calculations were conducted for 11 SZAs including 89.4°, 86.9°, 82.2°, 76.1°, 68.6°, 60.0°, 50.6°, 40.5°, 30.1°, 19.3°, and 8.5°. The results for the two largest SZAs are often excluded from the analysis, since radiative transfer calculations are less reliable at large SZAs.

Relationship between $APAR_{SFC}$ and $PAR_{TOA}\uparrow$

Following the method of Li et al. (1993a), the TOA-reflected PAR and the surface-absorbed PAR were computed for a variety of atmosphere–surface conditions and were then related for fixed SZAs. Since the SZA alters the pathlength of a photon traveling through a medium, it modifies the amount of solar energy absorbed and reflected by the medium. By fixing the SZA, this effect is eliminated. Figure 2 shows that $APAR_{SFC}$ and $PAR_{TOA}\uparrow$ have a very good linear relationship for the same SZA and varying cloud thickness. The significance of the relationship is that $APAR_{SFC}$ can be estimated from $PAR_{TOA}\uparrow$ without information on cloud thickness. For example, for a SZA of 8°, if the measured $PAR_{TOA}\uparrow$ is 300 W m^{-2}, a unique value of about 200 W m^{-2} is determined for $APAR_{SFC}$ regardless of cloud thickness. This technique is in stark contrast to that of $PAR_{SFC}\downarrow$, which critically depends on the knowledge of cloud optical thickness (cf. Pinker and Laszlo, 1992a). The linear relationship is driven primarily by the dependency of $APAR_{SFC}$ on $PAR_{TOA}\uparrow$ given by Eq. (3). When ozone amount and SZA are fixed, $APAR_{SFC}$ varies with $PAR_{TOA}\uparrow$ due to changes in cloud thickness. If $APAR_{ATM}$ were a constant, the slope of the relationship would be equal to −1. The actual value of the slope ranges from −1.03 to −1.01 as SZA changes from 8.5° to 82.2°. This can be explained by the coupling relationship between the atmospheric absorptance and planetary albedo for PAR, illustrated in Figure 3. The relationship is approximately linear, and its slope decreases with increasing SZA.

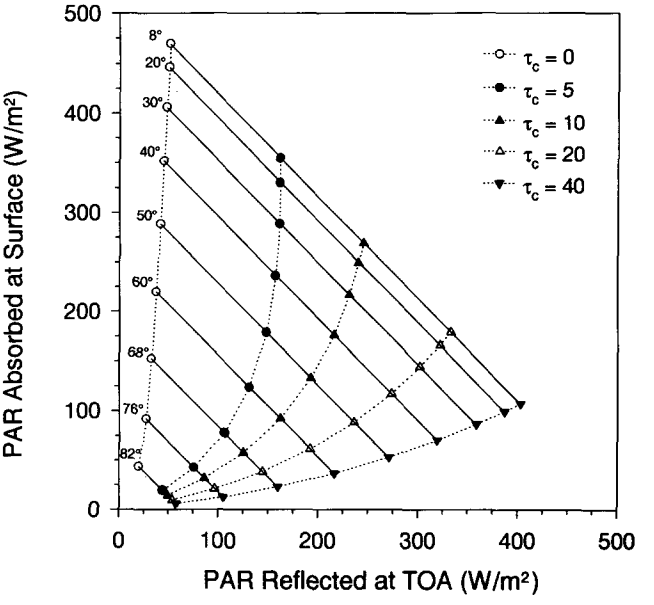

Figure 2. Relationship between the upwelling PAR at the TOA and the net PAR absorbed at the surface. Solid curves represent the linear regressions of the simulation results for different cloud optical thicknesses given by τ_c for the same SZAs. The simulations are for the midlatitude summer atmosphere with an ozone amount of 0.332 cm atm and a surface albedo of 5%.

SENSITIVITY STUDY

Ozone

Ozone is a major PAR absorber and thus a principal modulator of the relationship between $APAR_{SFC}$ and

Figure 3. Relationship between the atmospheric absorptance and the TOA albedo in the PAR wavelengths obtained from the same simulations as in Figure 2 for SZAs of 8° and 82°.

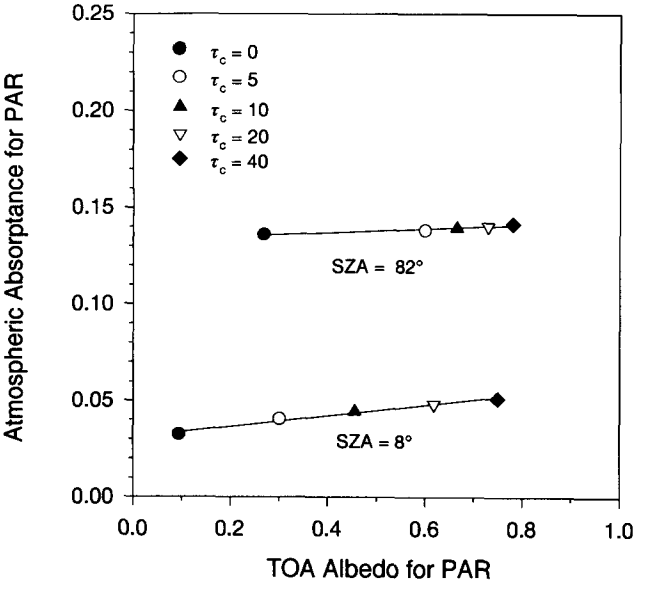

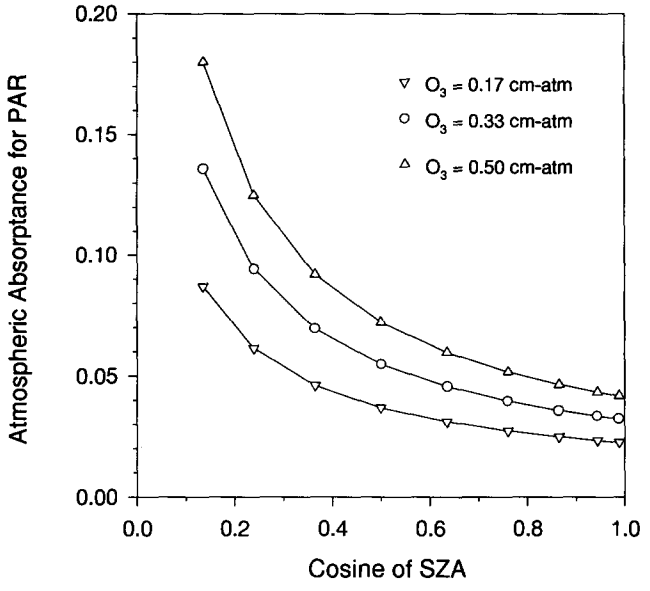

Figure 4. Variation in PAR atmospheric absorptance as a function of the cosine of the SZA for three ozone amounts.

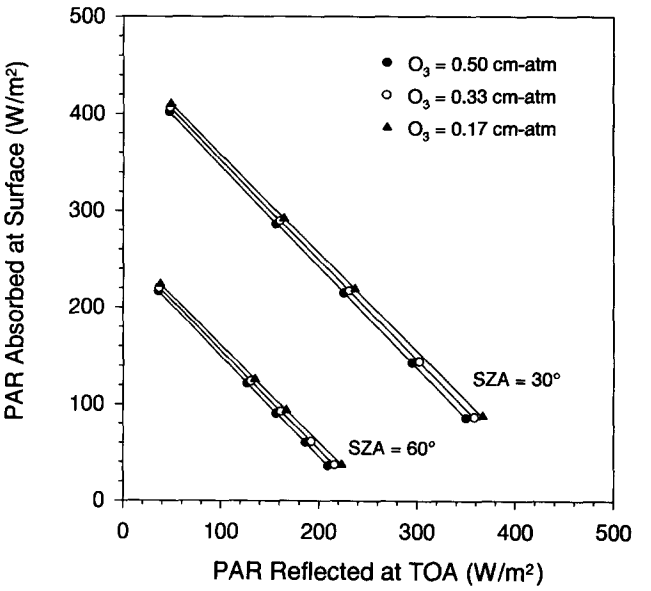

Figure 5. Same relationship as in Figure 2 but for different ozone contents for SZAs of 30° and 60°.

$PAR_{TOA}\uparrow$. Figure 4 shows the variation in PAR absorptance with ozone amount and SZA. The differences between the PAR absorptances for ozone amounts of 0.17 cm atm and 0.50 cm atm vary from 2% to 10%, depending on the SZA; 0.17 cm atm and 0.50 cm atm represent approximately the minimum and maximum ozone amounts observed in the upper atmosphere (Schoeberl, 1993). For an ozone content of 0.33 cm atm, an approximate ozone loading for a middle latitude summer atmosphere, the PAR absorptance ranges from 3% for the overhead sun to more than 13% for a SZA larger than 82.2°. The dependence of PAR absorptance on the SZA stems from the change in pathlength. As a result, ozone and SZA have significant impacts on the relationship between $APAR_{SFC}$ and $PAR_{TOA}\uparrow$, as is shown in Figure 5. Use of a constant ozone amount of 0.332 cm, when actual ozone amount varies from 0.17 cm atm to 0.50 cm atm, results in errors in the estimates of $APAR_{SFC}$ ranging from 10 W m^{-2} to 20 W m^{-2} for SZA = 30° and from 5 W m^{-2} to 10 W m^{-2} for SZA = 60°. It is seen from Figure 5 that the relationship is more sensitive to ozone for thick clouds than for thin clouds. The thicker the clouds, the more PAR is reflected for absorption by ozone, and thus the more sensitive the relationship is to the change of ozone amount.

Cloud Microphysics

The above analyses have been restricted to the same type of clouds with fixed cloud microphysics. Cloud optical properties are modified by cloud microphysics that is characterized mainly by the size distribution of the cloud droplets for pure liquid water clouds. Different cloud types have different size distributions (Stephens, 1979). Figure 6 simulates $APAR_{SFC}$ and $PAR_{TOA}\uparrow$ for four typical cloud types, namely, Nb, Sc, Cu, and St. The effective cloud radius, an important index of a size distribution, ranges from very small (4 μm) for stratus cloud to very large (31 μm) for nimbus. For the same cloud optical thickness, both $APAR_{SFC}$ and $PAR_{TOA}\uparrow$ change with cloud type. However, cloud type has no effect on their relationship, as the points corresponding

Figure 6. Same relationship as in Figure 2 but for different cloud types with cloud optical thickness ranging from 5 to 40.

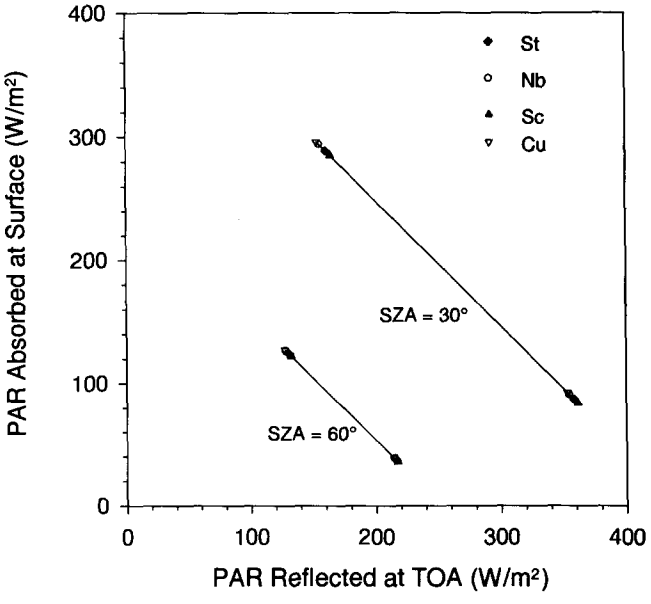

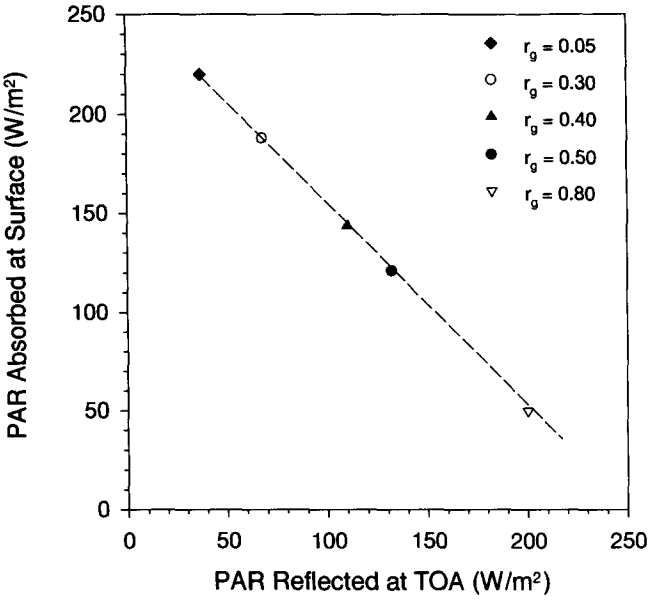

Figure 7. Same relationship as in Figure 2 but for different surface albedos given by r_g. The dashed line is taken from Figure 2.

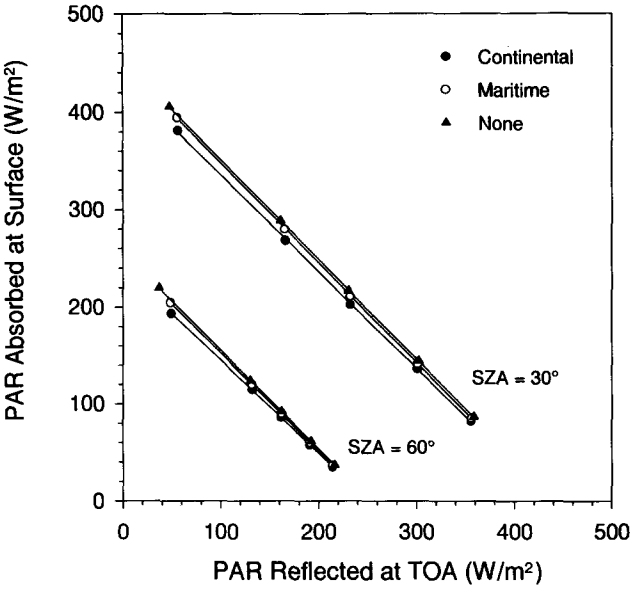

Figure 8. Same relationship as in Figure 2 but for three aerosol conditions, continental and maritime aerosols with optical thickness 0.225, and no aerosol.

to different cloud types lie along the same straight line. This is because the absorption extinction coefficients for all types of clouds are close to zero at the PAR wavelengths, whereas their scattering extinction coefficients are different. The finding suggests that retrieval of $APAR_{SFC}$ from $PAR_{TOA}\uparrow$ requires no information on cloud microphysics. Cloud optical thickness and droplet size distribution are the two most important cloud parameters. Knowledge of both is not needed for determining $APAR_{SFC}$ from $PAR_{TOA}\uparrow$.

Surface Albedo

Surface albedo is another parameter modifying the radiative transfer of PAR, which is also one of the input parameters in the $PAR_{SFC}\downarrow$ models. To investigate the effect of surface albedo on the relationship, $PAR_{TOA}\uparrow$ and $APAR_{SFC}$ were calculated for various surface albedos, and the results are given in Figure 7. As with clouds, Figure 7 suggests that $APAR_{SFC}$ is inversely correlated with $PAR_{TOA}\uparrow$. Hence, $APAR_{SFC}$ can be estimated from $PAR_{TOA}\uparrow$ without information on the surface albedo for a given atmospheric condition. This is not surprising, since changes in $PAR_{TOA}\uparrow$ and $APAR_{SFC}$ resulting from varying surface albedos are totally coupled. More important is the finding that the relationship formed by changing surface albedo is close to that by changing cloud thickness, implying that cloud and surface albedo have similar effects on the relationship. It can thus be deduced that cloud height has no effect on the relationship too, which has been confirmed by simulation results (not shown). Therefore, the relationship between $PAR_{TOA}\uparrow$ and $APAR_{SFC}$ is independent of cloud and surface conditions.

Aerosol

The optical properties (optical thickness, single scattering albedo, phase function) of an aerosol depend on its chemical composition, particle size distribution, vertical distribution, etc. Based on the optical properties, aerosols were classified into different types (WCP-112, 1986). The two most typical types are CON-I and MAR-I, representing continental aerosol and maritime aerosol, respectively. The former is much more absorbing than the latter, as the single scattering albedo over the PAR spectrum is around 0.89 for CON-I and 0.98 for MAR-I. Figure 8 illustrates the impact of aerosol type on the relationship between $PAR_{TOA}\uparrow$ and $APAR_{SFC}$ by fixing the aerosol optical depth at 0.225. Likewise, Figure 9 shows the impact of aerosol optical thickness for a fixed aerosol type (CON-I). The impacts indicated by the intervals between curves for the same $PAR_{TOA}\uparrow$ are considerable and vary with cloud optical thickness. The thicker the cloud, the smaller the effect of aerosol on the relationship is. Such a dependence on cloud thickness for aerosol is opposite to that for ozone. This is because aerosols are generally located below clouds, whereas ozone is above clouds. While 0.225 is supposed to represent the average aerosol loading for a rural continental atmosphere (WCP-112, 1986), the actual aerosol content may fluctuate substantially (D'Almeida et al., 1991). High aerosol loadings (greater than 0.5) are generally observed over deserts where vegetation is scarce so that almost no PAR is absorbed by canopy.

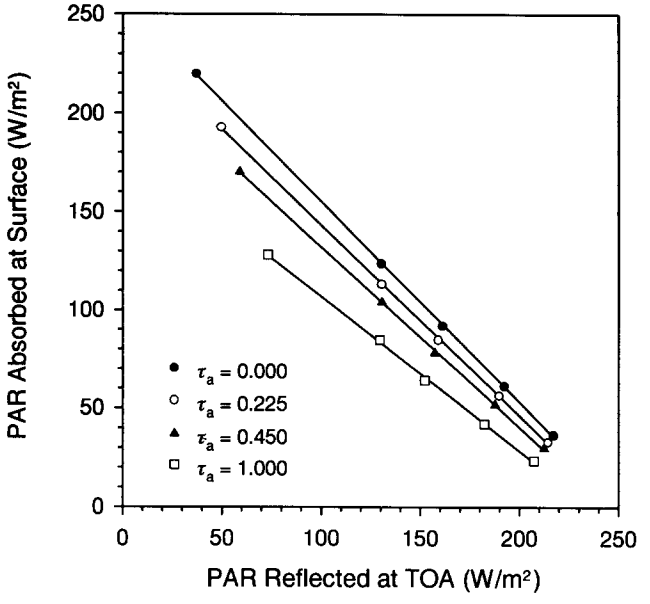

Figure 9. Same relationship as in Figure 2 but for a continental aerosol of varying optical thicknesses given by τ_a and an SZA = 60°.

Over vegetated land, aerosol content is relatively low and invariant.

PARAMETERIZATION

It follows from the sensitivity tests that the relationship between $APAR_{SFC}$ and $PAR_{TOA}\uparrow$ is linear and independent of cloud and surface conditions. The relationship is modified significantly by ozone and aerosol content by altering its slope and intercept. It is, therefore, possible to take their effects into account by parameterizing the slope and intercept as the functions of ozone and aerosol.

The linear relationship between $APAR_{SFC}$ and $PAR_{TOA}\uparrow$ can be expressed as

$$APAR_{SFC} = \alpha\, PAR_{TOA}\downarrow - \beta\, PAR_{TOA}\uparrow \tag{4}$$

where α and β are the coefficients of intercept and slope, respectively. $PAR_{TOA}\downarrow$ in Eq. (4) accounts for the dependency of the intercept on incoming PAR at the TOA, which is determined by

$$PAR_{TOA}\downarrow = \mu\, d^{-2}\, PAR_0, \tag{5}$$

where μ denotes the cosine of the SZA. PAR_0 is the extra-terrestrial irradiance in the PAR spectrum for the mean sun–earth distance, which constitutes 38%–39% of the total solar energy over the whole solar spectrum depending on solar spectral data (Thekaekara, 1974; Iqbal, 1983). d is the sun–earth distance given in astronomical units (a.u.) that varies through the year. d^{-2} can be approximated to an accuracy better than 10^{-4} by (Paltridge and Platt, 1976)

$$d^{-2} = 1.00011 + 0.034221 \cos\theta + 0.00128 \sin\theta + 0.000719 \cos 2\theta + 0.000077 \sin 2\theta, \tag{6}$$

$$\theta = 2\pi n/365 \tag{7}$$

where n is the day number ranging from 0 on 1 January to 364 on 31 December.

To understand the physical meaning of α and β and to establish parameterizations for computing their values, the following circumstances of increasing physical complexity are considered.

i. For a medium composed of solely conservative scatterers (e.g., atmospheric molecules for the Rayleigh scattering, cloud droplets for the Mie scattering), $APAR_{ATM} = 0$, it follows from Eq. (3) that

$$APAR_{SFC} = PAR_{TOA}\downarrow - PAR_{TOA}\uparrow. \tag{8}$$

Therefore, $\alpha = 1$ and $\beta = 1$.

ii. For a medium composed of pure absorbers (e.g., ozone only without backscattering), $PAR_{TOA}\uparrow = 0$, Eq. (4) becomes

$$APAR_{SFC} = PAR_{TOA}\downarrow - APAR_{ATM}. \tag{9}$$

Therefore, $\alpha = 1 - APAR_{ATM} / PAR_{TOA}\downarrow$, and β is undefined.

iii. For a medium composed of both scatterers and absorbers, determination of α and β is not so straightforward. It depends on how the scatterers and absorbers are distributed vertically and whether they interact with each other.

We start with a simple case where they are located in two separate layers, absorbers being above scatterers. Hence, there are no direct interactions between the absorbers and scatterers. This is a good assumption for an aerosol-free atmosphere which contains ozone as a major absorber which is situated well above the layer of scatterers including surface, cloud droplets, and the majority of atmospheric molecules. In this case, we can derive analytical expressions for α and β in terms of the ozone content, O_3, and the cosine of the SZA, μ (see the Appendix):

$$\alpha = \exp(-A\, O_3\, \mu^{-1}), \tag{10}$$

$$\beta = \exp(1.66\, A\, O_3), \tag{11}$$

where A denotes the effective ozone absorption coefficient over the PAR spectrum. α is the transmissivity of the PAR↓ through the ozone layer, and thus $\alpha \leq 1$. β is the reciprocal of the transmissivity for the $PAR_{TOA}\uparrow$ through the ozone layer, and thus $\beta \geq 1$. To also allow for minor absorption by other atmospheric constituents (e.g., oxygen), a correction term B is introduced to α, so that

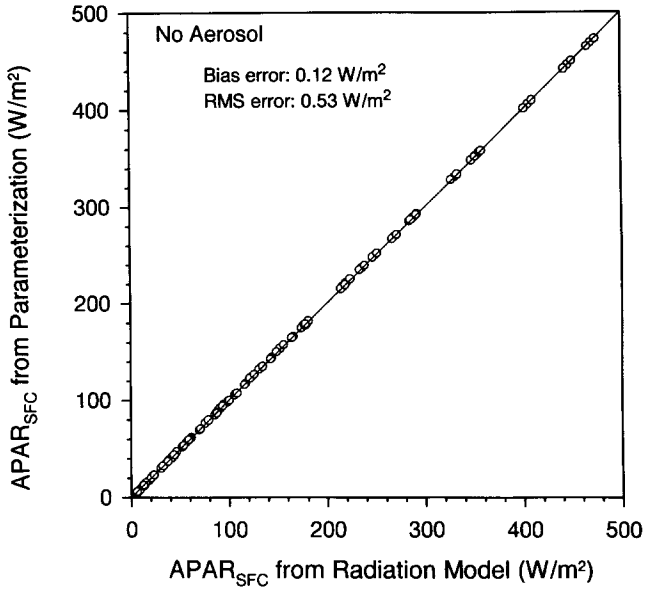

Figure 10. Comparison of the surface absorbed PAR simulated from a radiative transfer model and estimated with the parameterization given by Eq. (12) using the TOA upwelling PAR, ozone amount and SZA. The calculations are for 135 combinations of ozone content, cloud optical thickness and SZA without aerosol.

$$\mathrm{APAR_{SFC}} = [\exp(-A\,\mathrm{O_3}\,\mu^{-1}) - B]\,\mathrm{PAR_{TOA}}\downarrow - \exp(1.66\,A\,\mathrm{O_3})\,\mathrm{PAR_{TOA}}\uparrow . \quad (12)$$

A and B are equal to 0.050 and 0.015, respectively, for ozone amounts given in cm atm. They were determined with an optimization scheme by applying Eq. (12) to the results of radiative transfer calculations for 135 combinations of five cloud optical thickness (0, 5, 10, 20, 40), three ozone amounts (0.166 cm atm, 0.332 cm atm, and 0.498 cm atm) and nine SZAs less than 83°. It is worth noting that the value of A determined here coincides very well with the ozone absorption coefficient of 0.053 used by Eck and Dye (1991), following Goldberg and Klein (1980). Figure 10 compares the $\mathrm{APAR_{SFC}}$ simulated by the radiative transfer model and estimated from the parameterization of Eq. (12). The agreement is remarkable.

As expected, however, the parameterization cannot reproduce $\mathrm{APAR_{SFC}}$ well when aerosols are present. Figure 11 shows the same comparison as Figure 10 but with aerosols of varying amounts being added for the continental aerosol (a) and the maritime aerosol (b). Since the parameterization of Eq. (12) does not account for aerosol absorption, the $\mathrm{APAR_{SFC}}$ estimated from the parameterization is always larger than that modeled by radiative transfer model. For the continental aerosol, the overestimation in $\mathrm{APAR_{SFC}}$ amounts to 80 W $\mathrm{m^{-2}}$ when the aerosol optical thickness is 1 and the SZA is small. With the same optical thickness, the overestimation for the maritime aerosol is much less than that for the continental aerosol. It is thus concluded that a nonabsorbing aerosol has no effect on the parameterization.

Due to the complexities of the interactions between ozone, aerosol, clouds, and surface, it is difficult to derive an analytic expression accounting for the aerosol effects. An empirical correction term is thus introduced:

$$\Delta\mathrm{APAR_{SFC}} = C\tau_e[\mathrm{PAR_{TOA}}\downarrow - (D + E\mu)\mathrm{PAR_{TOA}}\uparrow] \times [\exp(-3\mu^2) + 1], \quad (13)$$

$$\tau_e = \tau[(1-\omega_i)/(1-\omega_c)]^F, \quad (14)$$

where the coefficients C, D, E, and F are tuned to be -0.168, 1.121, -0.348, and 0.845 respectively, following a procedure similar to the determination of A and B in Eq. (12) but using the results of radiative transfer simulations for different aerosols. ω is the energy weighted single scattering albedo over the PAR spectrum. The subscript i is for any type of aerosol and c for the continental aerosol. τ and τ_e denote actual and effective aerosol optical thicknesses, respectively. Since the optical properties of aerosols are relatively invariant throughout the PAR wavelengths, the values of ω, τ, and τ_e may be replaced by their corresponding values at 0.55 μm. At this wavelength, ω is equal to 0.891 for the continental aerosol and 0.978 for the maritime aerosol. While the correction was not derived based on the physics, it does satisfy a basic constraint that $\Delta\mathrm{APAR_{SFC}}$ is null when $\tau = 0$ or $\omega_i = 1$. For other values of τ and ω, $\Delta\mathrm{APAR_{SFC}}$ is always a negative quantity to be added to the $\mathrm{APAR_{SFC}}$ computed by Eq. (12). When the correction term is included, the comparison is much improved between the estimated and modeled $\mathrm{APAR_{SFC}}$, as is shown in Figure 12.

The complete parameterization scheme for computing $\mathrm{APAR_{SFC}}$ is given by

$$\mathrm{APAR_{SFC}} = a(\mu,\mathrm{O_3},\tau_e)\mathrm{PAR_{TOA}}\downarrow - \beta(\mu,\mathrm{O_3},\tau_e)\mathrm{PAR_{TOA}}\uparrow, \quad (15)$$

$$a(\mu,\mathrm{O_3},\tau_e) = -0.015 + \exp(-0.050\,\mathrm{O_3}\,\mu^{-1}) - 0.168\tau_e[\exp(-3\mu^2) + 1], \quad (16)$$

$$\beta(\mu,\mathrm{O_3},\tau_e) = \exp(0.083\,\mathrm{O_3}) - 0.168\tau_e(1.121 - 0.348\mu) \times [\exp(-3\mu^2) + 1]. \quad (17)$$

The dependencies of a and β on μ, ozone and aerosol are illustrated in Figures 13 and 14, respectively. a is always less than unity and depends strongly on μ, ozone, and aerosol. This is because a basically represents the transmissivity of the downwelling PAR. Without aerosol, β is always greater than 1, but it may be less than 1 when the aerosol loading reaches a certain amount.

THEORETICAL ANALYSES OF ERRORS

Errors Due to Parameterization

To get a more realistic estimate of the uncertainty in $\mathrm{APAR_{SFC}}$ arising from parameterization, 792 radiative

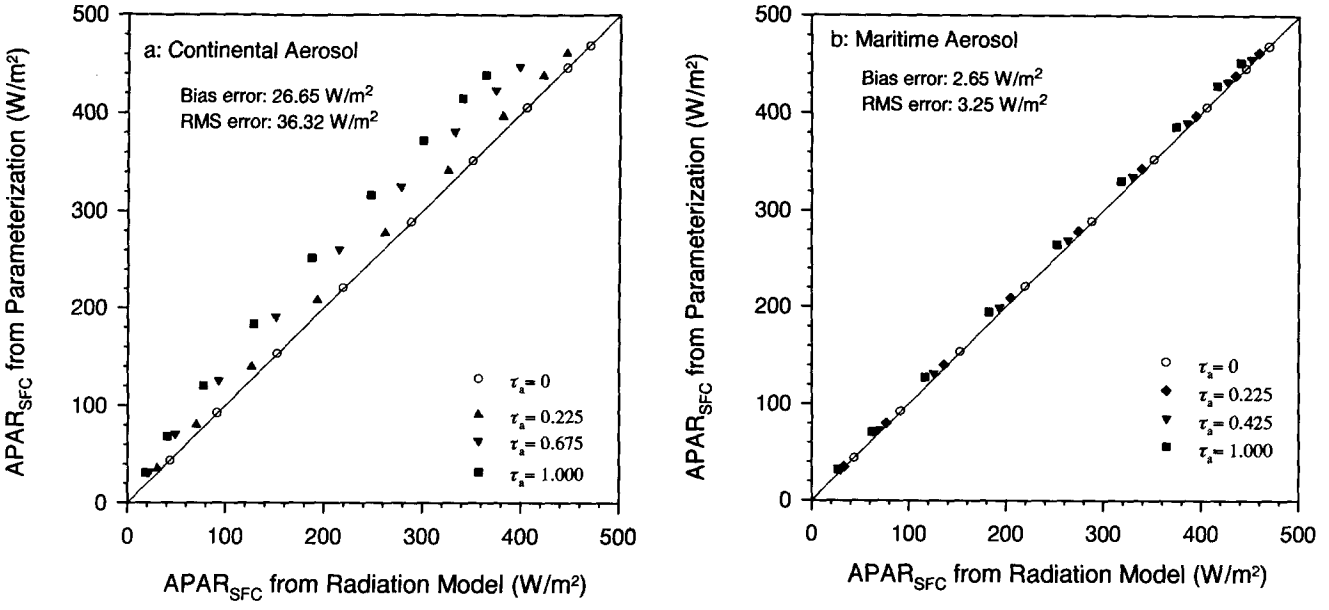

Figure 11. Same as Figure 10 but for a continental aerosol (a) and maritime aerosol (b) of varying optical thickness (τ_a) with a standard midlatitude summer atmosphere.

transfer runs were conducted at 9 SZAs for 88 conditions regarding the radiative properties of the atmosphere, cloud, and surface. The 88 cases represent partial combinations of four surface albedos (3–8%), 10 ozone amounts (0.166 cm atm to 0.498 cm atm), two aerosol types (continental and maritime), 17 aerosol optical thicknesses (0–1.0), 11 cloud optical thicknesses (0–40), and five cloud heights (1–12 km). The combinations represent a great variety of conditions that are likely to occur in reality. The majority of combinations were made manually and a few were generated by a random number generator. The diversity of the conditions under study leads to large variations in the simulated $PAR_{TOA}\uparrow$ and $APAR_{SFC}$ (see Fig. 15), which ensures a valid and revealing analysis of the parameterization error. Figure 16 presents the histogram of the differences in $APAR_{SFC}$ between model simulation and parameterization estimation. Note that 93% of the $APAR_{SFC}$ estimates are within 5 W m^{-2} of the simulated ones and 54% are within 1 W m^{-2}. Few estimates have absolute errors larger than

Figure 12. Same as Figure 11 except that the aerosol correction terms given by Eqs. (13)–(14) are added to the parameterization of Eq. (12).

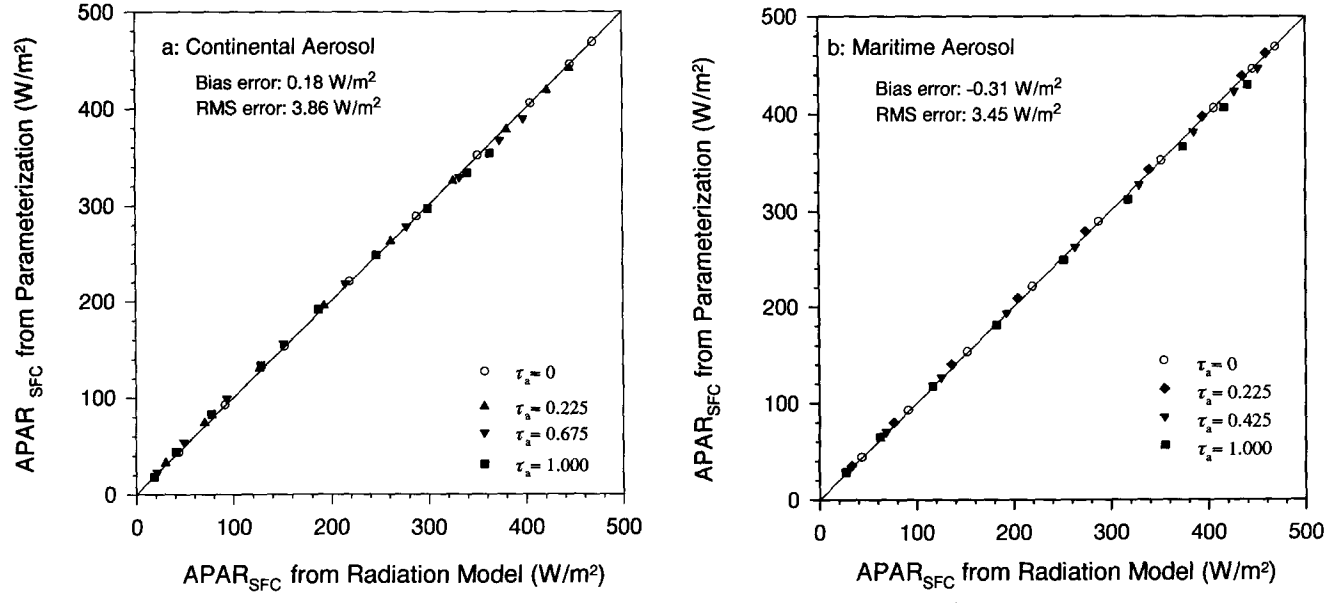

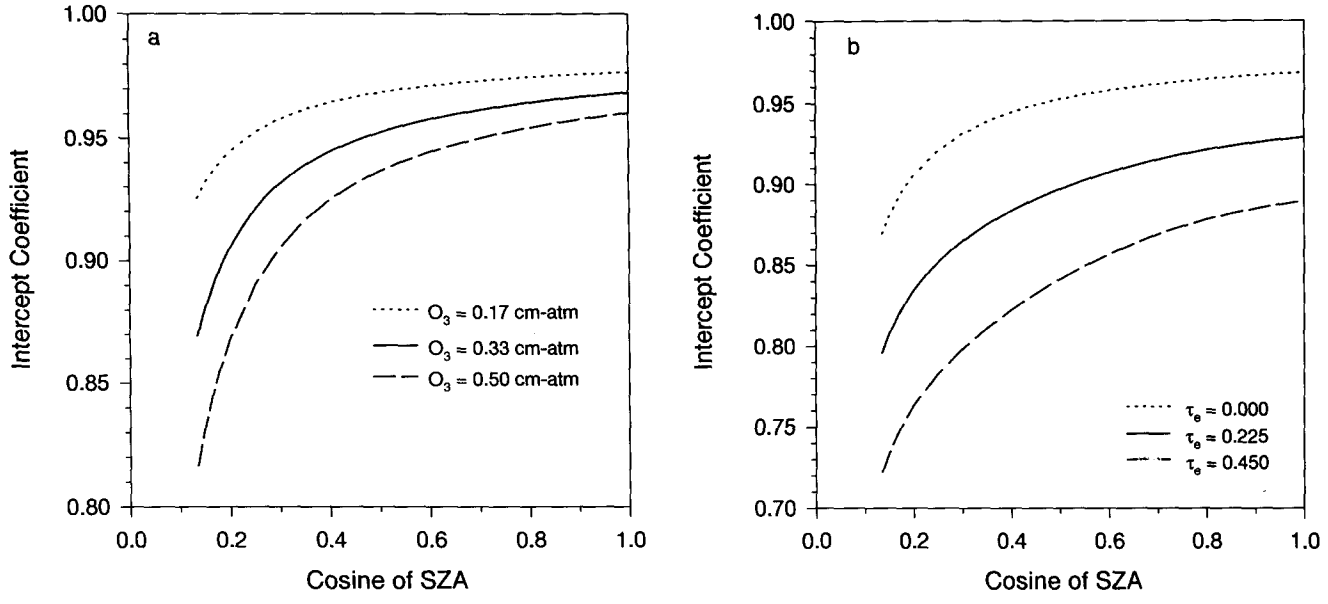

Figure 13. Variations in the intercept coefficient a given by Eq. (16) with the cosine of the SZA for different amounts of ozone (a) and aerosol (b).

10 W m^{-2}. The cases where absolute errors exceed 5 W m^{-2} generally occur for turbid atmosphere with τ greater than 0.5. These results demonstrate the robustness of the parameterization in terms of accuracy, simplicity, and universality.

Errors Due to Input Data

The errors shown in Figure 16 do not include those caused by inherent uncertainties in the input data. No doubt, the input parameters of the parameterization model contain uncertainties that contribute to the overall errors in the estimation of $APAR_{SFC}$. Among the four input parameters, only $PAR_{TOA}\downarrow$ is virtually error-free. Ozone is relatively stable and has been measured from space by TOMS on board the polar orbiting Nimbus-7 (Herman et al., 1991). The TOMS ozone data are accurate to within 2% or on the order of 0.01 cm atm (Varotsos and Cracknell, 1994). More than a decade worth of daily global ozone data are available (Schoeberl, 1993). Aerosol has moderate spatial and temporal variations but has not been monitored properly so far, especially over land. While a few techniques have been

Figure 14. Same as Figure 13 but for the slope coefficient β given by Eq. (17).

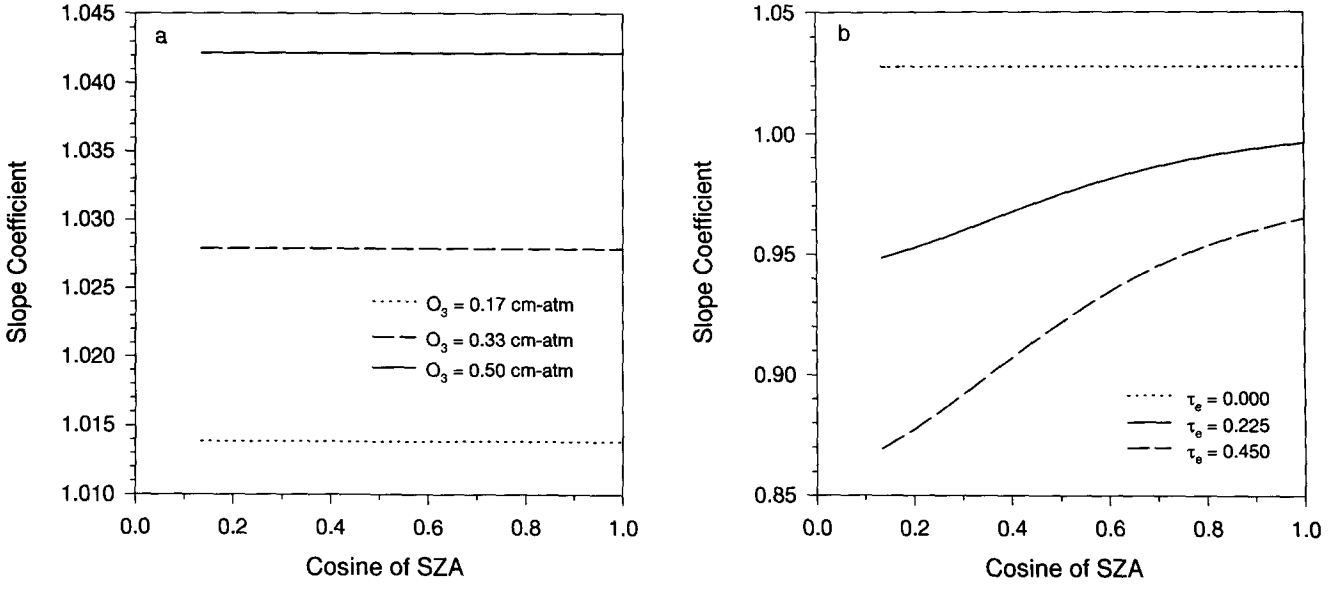

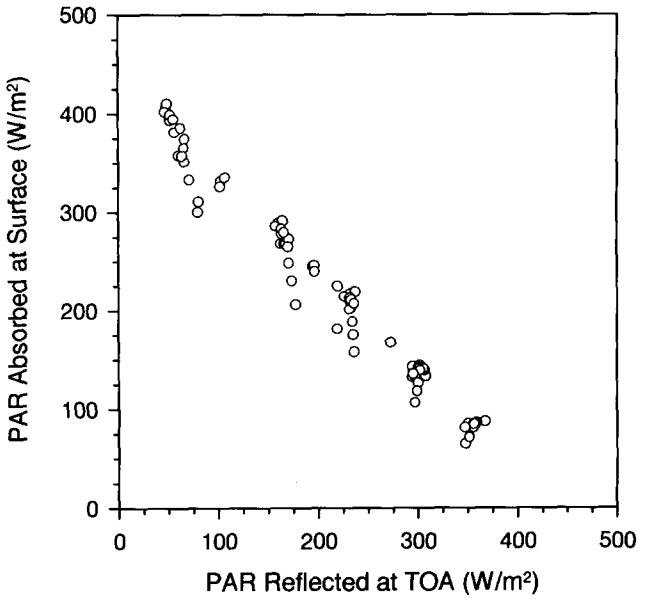

Figure 15. Scatter plot of the PAR fluxes absorbed at the surface and the PAR fluxes reflected at the top of the atmosphere. They were simulated by a radiative transfer model for 88 combinations of surface albedo, cloud optical thickness, aerosol, and ozone, varying over large ranges. The SZA was fixed at 30°.

proposed for retrieving aerosols over land, there are many constraints in their implementation (Holben et al., 1992). The absolute error in the retrieval of aerosol optical depth is 0.1–0.2, or 50–100% in terms of relative error. After the Earth Observing System (EOS) is deployed in the late 1990s, quality data on aerosol properties will be, hopefully, acquired by the Moderate Resolution Imaging Spectrometer (MODIS) (King et al., 1992), and the Multi-angle Imaging Spectro Radiometer (MISR) (Martpnchik and Diner, 1992). Before synergistic aerosol data become available, one may have to resort to aerosol climatology (D'Almeida et al., 1991). $PAR_{TOA}\uparrow$ is subject to the most dramatic changes with time and location due to the large variability of clouds. Fortunately, such a variation can be well monitored with a visible radiometer aboard weather satellites or resource satellites. These visible measurements can serve as surrogate $PAR_{TOA}\uparrow$ data after radiometric calibration, bidirectional correction, and spectral conversion. Radiometric calibration accounts for the post-launch degradation (Holben et al., 1990; Teillet et al., 1994). Bidirectional correction derives an upward irradiance or flux defined over the upward hemisphere from a reflected radiance observed from a specific direction by a satellite. Spectral conversion deals with the difference in spectral responsivity between PAR band and the bandpass of a radiometer, which will be addressed in detail in the next section. No doubt, all these processes add to the uncertainties in $PAR_{TOA}\uparrow$.

Figure 16. Histogram of the parameterization error defined as the difference between model-simulated surface absorbed PAR and that estimated from the parameterization given by Eqs. (15)–(17) for the combinations presented in Figure 15.

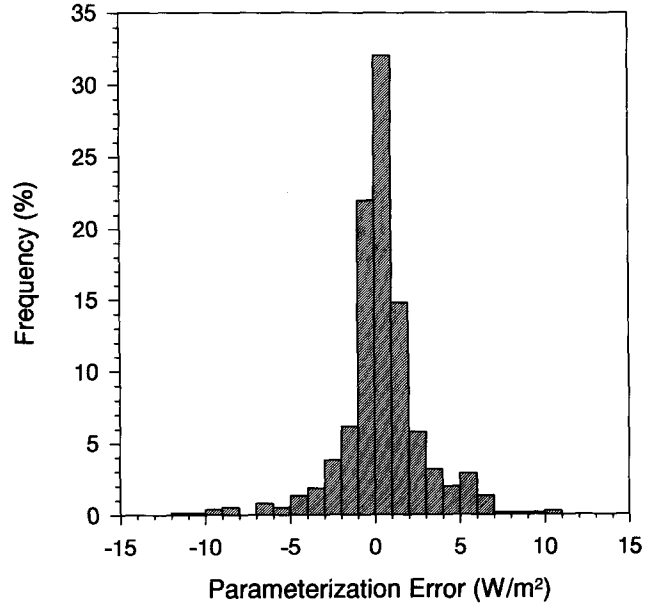

The errors in estimates of $APAR_{SFC}$ arising from the uncertainties in input data can be computed by differentiating the parameterizations given by Eqs. (15–17) with respect to ozone, aerosol, and $PAR_{TOA}\uparrow$:

$$\Delta APAR_{SFC}(O_3) = -\Delta O_3[0.050\mu^{-1}\exp(-0.050\,O_3\mu^{-1}) \times PAR_{TOA}\downarrow + 0.083\exp(0.083\,O_3) \times PAR_{TOA}\uparrow], \quad (18)$$

$$\Delta APAR_{SFC}(\tau_e) = -0.168\Delta\tau_e[\exp(-3\mu^2)+1] \times [PAR_{TOA}\downarrow + (1.121 - 0.348\mu) \times PAR_{TOA}\uparrow], \quad (19)$$

$$\Delta APAR_{SFC}(PAR_{TOA}\uparrow) = -\beta(O_3,\tau_e)\,\Delta PAR_{TOA}\uparrow, \quad (20)$$

$$\Delta APAR_{SFC}(\text{Total}) = \Delta APAR_{SFC}(O_3) + \Delta APAR_{SFC}(\tau_e) + \Delta APAR_{SFC}(PAR_{TOA}\uparrow), \quad (21)$$

where $\Delta APAR_{SFC}(O_3)$, $\Delta APAR_{SFC}(\tau_e)$, and $\Delta APAR_{SFC}(PAR_{TOA}\uparrow)$ denote the estimation errors in $APAR_{SFC}$ incurred due to the incorrect knowledge of ozone, aerosol, and $PAR_{TOA}\uparrow$, respectively. $\Delta APAR_{SFC}(\text{Total})$ is the total error in $APAR_{SFC}$ contributed by all input parameters. Note that β and the sums of the terms appearing in the square brackets on the right-hand sides of Eqs. (18) and (19) are always positive. Therefore, $\Delta APAR_{SFC}$ has the opposite sign to the uncertainties in the input data. If the uncertainties in the input data are known, one can readily determine the ensuing errors in the estimated $APAR_{SFC}$. These uncertainties depend on the data sets used and generally have large spatial and temporal variations.

Table 1. Information on Satellites and Visible Radiometers

Satellite	*Radiometer / Channel*	*50%-PRP[a] (μm)*	*Resolution*	*Frequency*
NOAA-11	AVHRR / 1	0.571–0.698	1.1 km	1 per day
GOES-8	VISSR / VIS	0.524–0.724	4 km	Every 30 min
SPOT-2	HRV / 1	0.506–0.591	20 m	
	HRV / 2	0.627–0.670	20 m	
LANDSAT-5	TM / 1	0.451–0.521	30 m	1 per 9 days
	TM / 2	0.526–0.615	30 m	1 per 9 days
	TM / 3	0.622–0.699	30 m	1 per 9 days

[a] *PRP* = percent response point.

ESTIMATION OF PAR_{TOA} FROM SATELLITE VISIBLE MEASUREMENTS

$PAR_{TOA}\uparrow$ is defined over the whole PAR spectrum from 400 nm to 700 nm, so that the parameterization developed is independent of radiometer. Thus, satellite sensors data must be converted to PAR bandpass values. The conversion is only feasible for a visible radiometer whose spectral coverage is close to the PAR spectrum. Visible channels are available from a series of weather satellites such as NOAA and GOES and land resource satellites such as LANDSAT and SPOT. Table 1 provides more detailed information about these instruments and satellites. Weather satellites provide daily measurements at moderate spatial resolution around the globe, while resource satellites provide measurements at high spatial resolutions but less frequently. Although any of these instruments can be used, in principle, for mapping $APAR_{SFC}$, few (e.g., AVHRR) are suitable for mapping $APAR_{CAN}$ due either to the lack of near-infrared channel or to the long revisiting period that prevents determining RPAR (Moreau and Li, 1996).

The spectral response of the sensor's bands is key to the conversion. The response is described by the spectral responsivity function (SRF), a wavelength-dependent function quantifying the sensitivity of a radiometer to incident radiation. SRF is often normalized so that it ranges from 0 to 1. The sensor's bandwidth measured by 50 percent response point (PRP) (see Table 1) varies considerably from one type of radiometer to another. While the SRFs of the same type of radiometers have similar shapes, they are never identical (Rossow et al., 1991). Hence, the conversion is best achieved by applying different conversion models to different radiometers, although the use of the same model for the same type of radiometer may be acceptable depending on how similar their SRFs are.

Satellite-observed visible irradiances can be simulated by

$$VIS_{TOA}\uparrow = \int_0^\infty R(\lambda) f(\lambda)\, d\lambda, \qquad (22)$$

where $f(\lambda)$ denotes an SRF in the visible band at a wavelength given by λ. R represents the reflected spectral irradiance at the sensor. In comparison, $PAR_{TOA}\uparrow$ is computed by

$$PAR_{TOA}\uparrow = \int_{400\text{ nm}}^{700\text{ nm}} R(\lambda)\, d\lambda. \qquad (23)$$

Apparently, both $VIS_{TOA}\uparrow$ and $PAR_{TOA}\uparrow$ depend on the radiative properties of the atmosphere–surface system. To gain an insight into their relationship, they were simulated under various conditions of the system with SRFs for different radiometers listed in Table 1. Figure 17 shows the relationships between $VIS_{TOA}\uparrow$ and $PAR_{TOA}\uparrow$ for NOAA-11, GOES-8, LANDSAT-5, and SPOT-2. Note that the visible irradiances presented in Figure 17 for LANDSAT and SPOT are the sums of the irradiances from multiple channels whose bandpasses are within the PAR spectrum. It follows that $PAR_{TOA}\uparrow$ is correlated well with $VIS_{TOA}\uparrow$ for all the sensors under study, and their relationships differ considerably among different types of radiometers. Even for the same type of radiome-

Figure 17. Simulated relationships between the upwelling PAR at the TOA and the upwelling fluxes filtered by the satellite visible sensors of four different radiometers aboard NOAA-11, GOES-8, LANDSAT-5, and SPOT-2.

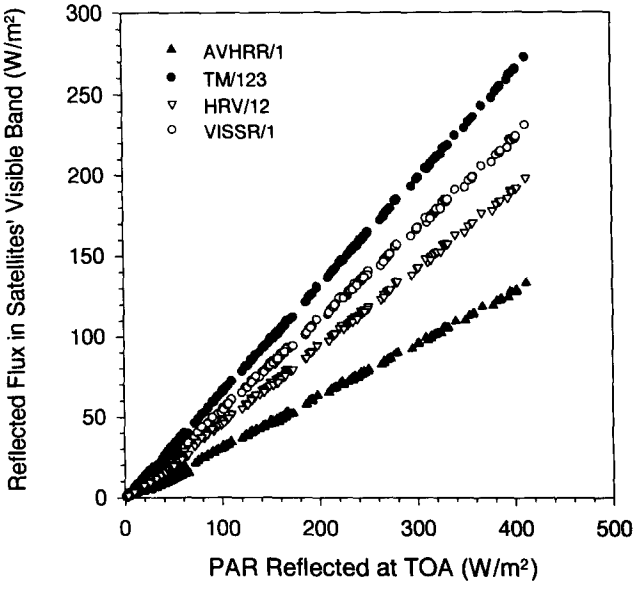

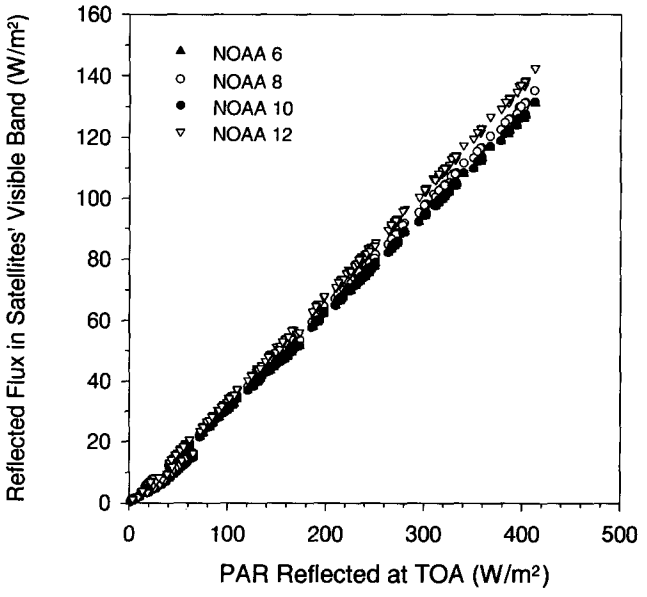

Figure 18. Same as Figure 17 but for the AVHRR aboard four different NOAA satellites.

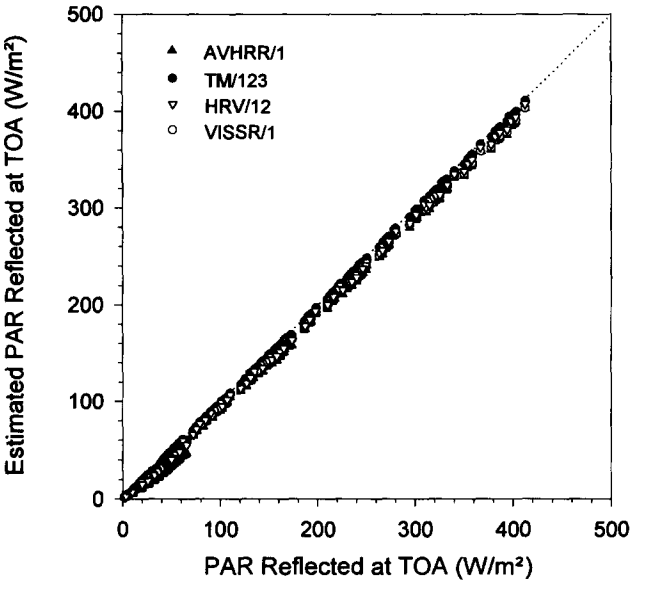

Figure 19. Simulated relationship between the reflected PAR at the TOA obtained from radiation model and estimated according to sensor's albedo for the same four types of radiometers as in Figure 17.

ter aboard different satellites, say, AVHRR / NOAA, the discrepancies in the relationship are appreciable (see Fig. 18). Therefore, the conversion model used to estimate $PAR_{TOA}\uparrow$ from $VIS_{TOA}\uparrow$ is given for each sensor with the following format:

$$PAR_{TOA}\uparrow = \sum_{i=1}^{n} C_i \, VIS_{TOA,i}\uparrow, \tag{24}$$

where n denotes the number of visible channels. The coefficients c_i are given in Table 2. Also included in Table 2 are the root mean square errors (RMSEs) of the conversion models. It appears that the conversion error decreases as the total bandwidth of the channels used increases. The best conversion is obtained for LANDSAT when TM Bands 1, 2, and 3 are all employed. This is not surprising since their combined spectral coverage approximates the PAR band.

Satellite data may be given in the units of albedo instead of radiance following radiometric calibration and bidirectional correction (Cihlar et al., 1994). Satellite albedo ρ is defined as

$$\rho = \frac{\int_0^\infty R(\lambda) f(\lambda)\, d\lambda}{\int_0^\infty I(\lambda) f(\lambda)\, d\lambda}, \tag{25}$$

where I denotes instantaneous solar flux incident at the TOA. From ρ, upwelling PAR at the TOA can be approximated by

$$PAR_{TOA}\uparrow = \rho \, PAR_{TOA}\downarrow, \tag{26}$$

where $PAR_{TOA}\uparrow$ is given by Eq. (5). Figure 19 compares the $PAR_{TOA}\uparrow$ estimated from ρ to the $PAR_{TOA}\uparrow$ simulated by model for the four types of radiometers given in

Table 2. Conversion Coefficients for Different Sensors Used in Eq. (24)

Satellite	*Radiometer / Channel*	c_1	c_2	c_3	*RMSE*[a] ($W\ m^{-2}$)
NOAA6	AVHRR / 1	3.120	–	–	5.77
NOAA7	AVHRR / 1	3.224	–	–	5.64
NOAA8	AVHRR / 1	3,103	–	–	5.22
NOAA9	AVHRR / 1	3.087	–	–	5.59
NOAA10	AVHRR / 1	3.198	–	–	5.79
NOAA11	AVHRR / 1	3.176	–	–	5.73
NOAA12	AVHRR / 1	2.945	–	–	5.86
GOES-5	VISSR / VIS	2.043	–	–	2.75
GOES-6	VISSR / VIS	2.089	–	–	3.10
GOES-7	VISSR / VIS	2.625	–	–	2.39
GOES-8	VISSR / VIS	1.812	–	–	2.49
SPOT2	HRV / 1,2	5.513	1.726	–	1.95
LANDSAT5	TM / 1,2,3	2.350	1.277	0.839	0.15

[a] RMSE = root mean square error.

Table 1. For LANDSAT and SPOT, the mean albedos from multiple channels are used. The comparison is very encouraging, as the points distribute closely along the 1:1 line. The standard deviation of the differences is only 3.91 W m^{-2}. In comparison to Eq. (24), Eq. (26), is independent of radiometer. This is because ρ does not strongly depend on wavelength over the PAR spectrum.

PRELIMINARY EXPERIMENTAL VALIDATION

Note that the algorithm introduced above was solely based on radiative transfer simulations and no observational data were used to tune the algorithm, which assures general utility of the algorithm. Observations are, however, needed to validate the model-based algorithm. For a preliminary validation, data collected during the First ISLSCP Field Experiment (FIFE) were employed. The FIFE was conducted near Manhattan, Kansas, in 1987 and 1989 (Sellers et al., 1992). All the parameters required for validation were measured during the FIFE and the data were published in five volumes of CD-ROMs. They include ozone, aerosol, satellite imageries, and surface downwelling and upwelling PAR. The imageries of NOAA 9, 10, and 11, SPOT, and LANDSAT were processed to obtain TOA visible reflectance (ρ) data. Unfortunately, no raw TOA data from GOES were archived in the FIFE CD-ROMs. Postlaunch calibration were applied to NOAA / AVHRR data, following the methods proposed by Rao and Chen (1994) for NOAA 9 and 11 and Teillet and Holben (1994) for NOAA 10. No bidirectional correction was carried out. The satellite reflectance data were collocated with surface observations by selecting those pixels that encompass the sites of surface PAR observations. The surface measurements of PAR were obtained by two teams from the Kansas State University (KSU) and the University of Nebraska at Lincoln (UNL). They placed LI-COR quantum sensor above the top of canopies at 25–50 locations within a FIFE site of 200×200 m^2 to provide spatially averaged PAR measurements (Demetriades-Shah et al., 1992). To match surface and satellite observations in time, the PAR measurements having SZAs within 5° of the SZA of a satellite measurement on the same side with respect to local noon were further averaged. This is equivalent to time differences ranging from less than 10 min to more than 20 min, depending on the time of day. Such a temporal averaging may compensate for, to some extent, the discrepancy in spatial coverage between satellite and surface observations and alleviate the effect of data noise. There were originally 112 pairs of downwelling and upwelling PAR irradiance measurements. After matching with satellite data, only nine pairs of data retained were reasonably close to satellite data in time and space. No surface PAR measurements could be matched to the satellite data from NOAA 9 and LANDSAT.

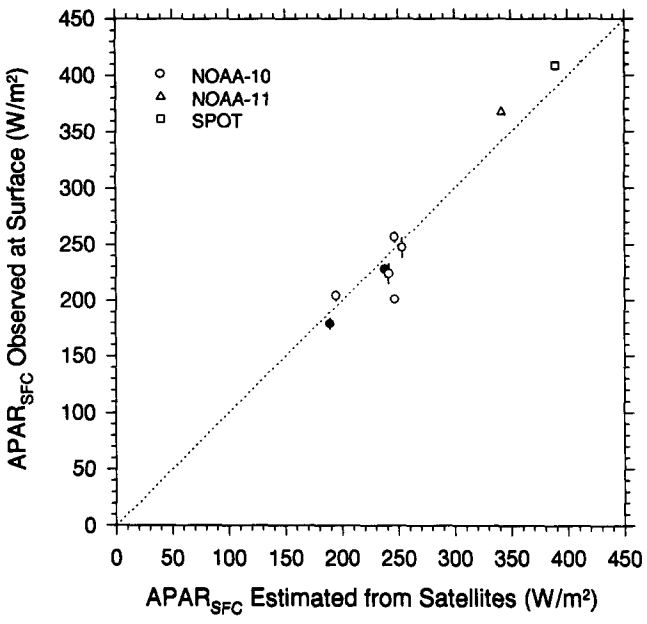

Figure 20. Comparison between observed and estimated surface absorbed PAR. Open and solid points represent the ground-based PAR measurements during the FIFE made by the teams from the University of Nebraska at Lincoln and the Kansas State University, respectively. The shapes of the symbols denote spacecraft. The bars on the plot denote the standard deviations of the surface measurements of $APAR_{SFC}$.

The algorithm was then applied to the satellite reflectance data, together with aerosol optical depth measurements at a wavelength nearest to 550 nm and a constant ozone amount of 0.3 cm atm. Ozone fluctuated very little (typically less than 10%) during the period of the data used here. In contrast, aerosol optical depth changed more drastically, ranging from less than 0.05 to larger than 0.3 (Bruegge et al., 1992). A continental aerosol type (CON-I) was assumed, since no single scattering data were available from the FIFE CD-ROMs. The amounts of $APAR_{SFC}$ estimated from satellite-based $PAR_{TOA}\uparrow$ with the parameterization are then compared to the corresponding surface observations. Good agreement is seen from Figure 20, bias and standard errors being -2.7 W m^{-2} and 21.9 W m^{-2}, respectively. Half of the compared data agree to within 10 W m^{-2}. The discrepancies shown in Figure 20 are expected to be comparable to the errors resulting from the uncertainties of input data and matching errors. The largest negative difference of -45 W m^{-2} corresponds to a surface measurement that differs most in time from a satellite observation (22 min). Spatial difference in the coverage of satellite and surface measurements is another major source of matching error. Note that the minimal footprint of an AVHRR pixel is 1.1 km, while

surface data are averages over areas of less than 200×200 m^2. Such a spatial matching error is expected to be larger for $APAR_{SFC}$ than for $PAR_{SFC}\downarrow$, since the former is modified by both the sky and surface conditions, whereas the latter is affected by the sky condition only.

Nevertheless, the estimation of $APAR_{SFC}$, shown here is somewhat superior to that of $PAR_{SFC}\downarrow$ as reported in the literatures. For example, Frouin and Gautier (1990) compared their estimates of $PAR_{SFC}\downarrow$ from GOES against the FIFE observations of $PAR_{SFC}\downarrow$. They obtained a bias error of 4.0 W m^{-2} and a standard error of 41.9 W m^{-2} for the comparison of a similar time scale (half-hour average) and 1.4 W m^{-2} and 8.2 W m^{-2} for the daily mean comparison. The significant decreases in the errors with time scale arise from the fact that many of the errors are of random nature, which tends to be canceled out by averaging. If the same factors of error reduction were assumed, the bias and standard errors in the daily mean estimates of $APAR_{SFC}$ would diminish to near 0 and less than 5 W m^{-2}, respectively. For a monthly mean comparison, the standard error should decrease further owing to the increased time scale of averaging. In comparison, the standard error in the monthly mean estimates of $PAR_{SFC}\downarrow$ is about 9 W m^{-2} (or 22.7 MJ m^{-2} in terms of monthly total amount) obtained by Goward et al. (1994) and 5 W m^{-2} (or 13,510 KJ m^{-2} in terms of monthly total amount) by Eck and Dye (1991). In addition to the improved accuracy, the current method is easy to implement with relatively few number of input parameters, compared to techniques for retrieving $PAR_{SFC}\downarrow$.

SUMMARY

The study proposed an alternative means of remote sensing the amount of photosynthetically active radiation (PAR) absorbed by a canopy ($APAR_{CAN}$). So far, $APAR_{CAN}$ has been derived from the incoming PAR at the surface ($PAR_{SFC}\downarrow$) and the fraction of PAR (FPAR) intercepted by a green canopy. Retrieval of $PAR_{SFC}\downarrow$ from satellite depends crucially on the accuracy of the inferred cloud parameters. Unfortunately, determination of cloud parameters from satellite measurements is still a difficult task and prone to large uncertainties.

The method introduced here circumvented the difficulties associated with cloud retrieval. Since clouds have negligible absorption over the PAR spectrum (400–700 nm), it is easier and more accurate to determine the total amount of PAR absorbed at the surface than the downwelling PAR. By virtue of radiative transfer simulations in the atmosphere, the relationship between the upwelling PAR at the top of the atmosphere (TOA) and the PAR absorbed at the surface is explored extensively. The two quantities are linearly related for a variety of atmospheric, cloud, and surface conditions. The relationship is independent of cloud properties (thickness, microphysics, height, etc.) and surface albedo, but depends on the solar zenith angle, ozone, and aerosol. Their effects were accounted for by parameterizing the slope and intercept of the relationship as functions of these variables. The parameterization was tested by comparing the simulated values of $APAR_{CAN}$ from the detailed radiation model with those estimated from the parameterization. The differences are generally within 5 W m^{-2}, which do not include the errors caused by the uncertainties in the input data. Since the upwelling PAR at the TOA in the parameterization was defined over the complete region of the PAR spectrum, spectral conversion is needed for using satellite filtered visible measurements. Conversion models were developed in terms of both radiance and albedo. The former is sensor specific, whereas the latter is quite universal. The whole procedure of this method was validated using observational data from FIFE. Preliminary results show that the PAR adsorbed at the surface can be estimated more accurately than the downwelling PAR at the surface. Once the total amount of PAR absorbed at the surface is known, the proportion of which absorbed by green canopy only can be determined using a method described in Moreau and Li (1996).

We thank J. Cihlar and P. Teillet for useful discussions, J. Chen and G. Fedosejevs for careful review of the draft, K. Masuda for providing the doubling-adding radiative transfer code, C. Langham for editorial assistance, and B. Markham for help in using satellite data. The FIFE science teams and Information System staff contributed to the collection and distribution of FIFE data.

APPENDIX: DERIVATION OF THE PARAMETERIZATION COEFFICIENTS

From Eqs. (3) and (4), we have

$$APAR_{ATM} = (1 - a)PAR_{TOA}\downarrow - (1 - \beta)PAR_{TOA}\uparrow. \quad (A1)$$

The relationship between atmospheric absorptance APAR and TOA reflectance r over the PAR spectrum is obtained by dividing Eq. (A1) over $PAR_{TOA}\downarrow$:

$$APAR = (1 - a) - (1 - \beta)r. \quad (A2)$$

For a simple two-layer model atmosphere, with a purely absorbing layer of ozone being above a conservative scattering layer of air molecules, clouds, and surface, a and r can be expressed as

$$APAR = (1 - \tau_1) + r_{cs}\tau_1(1 - \tau_2), \quad (A3)$$

$$r = r_{cs}\tau_1\tau_2, \quad (A4)$$

where τ_1 and τ_2 denote the transmittances of the upper layer for downwelling direct PAR and upwelling diffuse PAR, respectively. r_{cs} is the albedo of the second layer.

τ_1 and τ_2 are determined by ozone amount, O_3, and the cosine of the SZA, μ:

$$\tau_1 = \exp(-A\,O_3\,\mu^{-1}), \quad \text{(A5)}$$

$$\tau_2 = \exp(-1.66\,A\,O_3), \quad \text{(A6)}$$

Where A is the broadband ozone absorption coefficient over the PAR spectrum; 1.66 is the diffusivity factor. From Eqs. (A3)–(A4), APAR is related to r by

$$\text{APAR} = (1-\tau_1) - (1-\tau_2^{-1})r. \quad \text{(A7)}$$

Comparing Eq. (A7) with Eq. (A2), we have

$$\alpha = \tau_1 = exp(-A\,O_3\,\mu^{-1}), \quad \text{(A8)}$$

$$\beta = \tau_2^{-1} = \exp(1.66\,A\,O_3). \quad \text{(A9)}$$

REFERENCES

Asrar, G., Fuchs, M., Kanemasu, E. T., and Hatfield, J. L. (1984), Estimating absorbed photosynthesis radiation and leaf area index from spectral reflectance in wheat, *Agron. J.* 76:300–306.

Baker, K., and Frouin, R. (1987), Relation between photosynthetically available radiation and total insolation at the ocean surface under clear skies, *Limnol. Oceanogr.* 32: 1370–1377.

Budyko, M. I. (1980), *Global Ecology*, Progress Publishers, Moscow.

Braslau, N., and Dave, J. V. (1973), Effects of aerosols on the transfer of solar energy through realistic model atmospheres. Part I: Non-absorbing aerosols. *J. Appl. Meteorol.* 12:601–615.

Bruegge, C. J., Halthore, R. N., Markham, B., Spanner, M., and Wrigley, R. (1992), Aerosol optical depth retrievals over the Konza Prairie, *J. Geophys. Res.* 97:18,743–18,758.

Cihlar, J., Manak, D., and Voisin, N. (1994), AVHRR bidirectional reflectance effects and composite, *Remote Sens. Environ.* 48:77–88.

D'Almeida, G. A., Koepke, P., and Shettle, E. P. (1991), *Atmospheric Aerosols: Global Climatology and Radiative Characteristics*, A. Deepak, Hampton, VA, 561 pp.

Demetriades-Shah, T. H., Kanemasu, E. T., and Flitcroft, I. D. (1992), Comparison of ground-based measurements of the fraction of photosynthetically active radiation intercepted by tallgrass prairie, *J. Geophys. Res.* 97:18,947–18,950.

Dye, D. G., and Goward, S. N. (1993), Photosynthetically active radiation absorbed by global land vegetation in August 1984, *Int. J. Remote Sens.* 14:3361–3364.

Eck, T. F., and Dye, D. G. (1991), Satellite estimation of incident photosynthetically active radiation using ultraviolet reflectance, *Remote Sens. Environ.* 38:135–146.

Frouin, R., and Gautier, C. (1990), Variability of photosynthetically available and total solar irradiance at the surface during FIFE: a satellite description, in *Proc. Symp. 1st ISLSCP Field Exp.* 7–9 Feb. 1990, Anaheim, CA, Am. Meteorol. Soc., Boston, pp. 98–104.

Frouin, R., and Pinker, R. T. (1995), Estimating photosynthetically active radiation (PAR) at the earth's surface from satellite observations, *Remote Sens. Environ.* 51:98–107.

Gautier, C., Diak, G., and Masse, S. (1980), A simple physical model to estimate incident solar radiation at the surface from the GOES satellite data, *J. Appl. Meteorol.* 19:1005–1012.

Goldberg, B., and Klein, W. H. (1980), A model for determining the spectral quality of daylight on a horizontal surface at any geographical location, *Solar Energy* 24:351–357.

Goward, S. N., and Huemmrich, K. F. (1992), Vegetation canopy PAR absorptance and the normalized different vegetation index: An assessment using the SAIL model, *Remote Sens. Environ.* 39:119–140.

Goward, S. N., Waring, R. H., Dye, D. G., and Yang, J. (1994), Ecological remote sensing at OTTER: satellite macroscale observation, *Ecol. Appl.* 4(2):332–343.

Herman, J., Hudson, R., McPeters, R., et al. (1991), A new self calibration method applied to TOMS / SBUV backscattered ultra-violet data to determine long-term global ozone change, *J. Geophys. Res.* 96:7531–7545.

Holben, B. N., Kaufman, Y. J., and Kendall, J. D. (1990), NOAA-11 AVHRR visible and near-IR inflight calibration, *Int. J. Remote Sens.* 8:1511–1519.

Holben, B. N., Vermote, E., Kaufman, Y. J., Tanré, D., and Kalb, V. (1992), Aerosol retrieval over land from AVHRR data—application for atmospheric correction, *IEEE Trans. Geosci. Remote Sens.* 30:212–222.

Iqbal, M. (1983), *An Introduction to Solar Radiation*, Academic, New York, 390 pp.

King, M. D., Kaufman, Y. J., Menzel, W. P., and Tanre, D. (1992), Remote sensing of cloud, aerosol, and water vapour properties from the moderate resolution imaging spectrometer (MODIS), *IEEE Trans. Geosci. Remote Sens.* 30:2–27.

Li, Z. (1995), Intercomparison between two satellite-based products of net surface shortwave radiation, *J. Geophys. Res.* 100:3221–3232.

Li, Z., and Leighton, H. G. (1993), Global climatology of solar radiation budgets at the surface and in the atmosphere from 5 years of ERBE data, *J. Geophys. Res.* 98:4919–4930.

Li, Z., Leighton, H. G., Masuda, K., and Takashima, T. (1993a), Estimation of SW flux absorbed at the surface from TOA reflected flux, *J. Climate* 6:317–330.

Li, Z., Leighton, H. G., and Cess, R. D. (1993b), Surface net solar radiation estimated from satellite measurements: comparison with tower observations, *J. Climate* 6:1764–1772.

Li, Z., Whitlock, C., and Charlock, T. (1995), Assessment of the global monthly mean surface insolation estimated from satellite measurements using the Global Energy Balance Archive data, *J. Climate* 8:315–328.

Los, S. O., Justice, C. O., and Tucker, C. J. (1994), A global 1° by 1° NDVI data set for climate studies derived from the GIMMS continental NDVI data, *Int. J. Remote Sens.* 15:3493–3518.

Martonchik, J. V., and Diner, D. J. (1992), Retrieval of aerosol optical properties from multi-angle satellite imagery, *IEEE Trans. Geosci. Remote Sens.* 30:223–230.

Masuda, K., Leighton, H. G, and Li, Z. (1995), A new parameterization for the determination of solar flux absorbed at the surface from satellite measurements, *J. Climate* 8:1615–1629.

Monteith, J. L. (1971), Climate variation and the growth of crops, *J. Roy. Meteorol. Soc.* 107:749–774.

Moreau, L., and Li, Z. (1996), A new approach for estimating photosynthetically active radiation absorbed by canopy from space. II: Proportion of canopy absorption, *Remote Sens. Environ.* 55:192–204.

Myneni, R. B., Asrar, G., Tanré, D., and Choudhury, B. J. (1992), Remote sensing of solar radiation absorbed and reflected by vegetated land surfaces, *IEEE Trans. Geosci. Remote Sens.* 30:302–314.

Paltridge, G. W., and Platt, C. M. R. (1976), *Radiative Processes in Meteorology and Climatology*, Elsevier, Amsterdam, 320 pp.

Pinker, R. T., and Laszlo, I. (1992a), Global distribution of photosynthetically available radiation as observed from satellites, *J. Climate* 5:56–65.

Pinker, R., and Laszlo, I. (1992b), Modelling surface solar irradiance for satellite applications on a global scale, *J. Appl. Meteorol.* 31:194–211.

Pinker, R. T., Frouin, R., and Li, Z. (1995), A review of satellite methods to derive surface shortwave irradiance, *Remote Sens. Environ.* 51:108–124.

Pinter, P. J., Jr. (1993), Solar angle independence in the relationship between absorbed PAR and remotely sensed data for Alfalfa, *Remote Sens. Environ.* 46:19–25.

Rao, C. R. N. (1984), Photosynthetically active components of global solar radiation: Measurements and model computations, *Arch. Meteorol. Geophys. Biocl. Ser. B* 34:353–364.

Rao, C. R. N., and Chen, J. (1994), Post-launch calibration of the visible and near infrared channels of the Advanced Very High Resolution Radiometer on NOAA-7, -9, and -11 spacecraft, NOAA Tech. Rep., NESDIS 78, Washington, DC, 22 pp.

Rossow, W., Garder, L., Lu, P., and Walker, A. (1991), *International Satellite Cloud Climatology Project (ISCCP) Documentation of Cloud Data*, World Meteorological Organization, WMO / TD-No. 266, 76 pp.

Schmetz, J. (1989), Towards a surface radiation climatology: retrieval of downward irradiance from satellites. *Atmos. Res.* 23:287–321.

Schoeberl, M. R. (1993), Stratospheric ozone depletion, in *Atlas of Satellite Observations Related to Global Change* (R. J. Gurney, J. L. Foster, and C. L. Parkinson, Eds.), Cambridge University Press, Cambridge, pp. 59–65.

Sellers, P. J. (1985), Canopy reflectance, photosynthesis and transpiration, *Int. J. Remote Sens.* 6:1335–1372.

Sellers, P. J. (1987), Canopy reflectance, photosynthesis and transpiration. II. The role of biophysics in the linearity of their independence, *Remote Sens. Environ.* 21:143–183.

Sellers, P. J., Mintz, Y., Sud, Y., and Dalcher, A. (1986), A simple biosphere model (SiB) for use within general circulation models, *J. Atmos. Sci.* 43:505–531.

Sellers, P. J., Hall, F. G., Asrar, G., Strebel, D. E., and Murphy, R. E. (1992), An overview of the first International Satellite Land Surface Climatology Project (ISLSCP) Field Experiment (FIFE), *J. Geophys. Res.* 97:18,345–18,371.

Sellers, P. J., Los, S. O., Tucker, C. J., et al. (1994), A global 1° by 1° NDVI data set for climate studies. Part 2: The generation of global fields of terrestrial biophysical parameters from the NDVI, *Int. J. Remote Sens.* 15:3519–3545.

Stephens, G. L. (1979), Tech. Paper No. 36: Optical properties of eight water cloud types, 36 pp. [Available from CSIRO Division of Atmospheric Physics.]

Tarpley, J. D., Schneider, S. R., and Money, R. L. (1984), Global vegetation indices from the NOAA-7 meteorological satellite, *J. Climate Appl. Meteorol.* 23:491–494.

Teillet, P. M., and Holben, B. N. (1994), Towards operational radiometric calibration of NOAA AVHRR imagery in the visible and near-infrared channels, *Can. J. Remote Sens.* 20: 1–10.

Thekaekara, M. P. (1974), Extraterrestrial solar spectrum, 3000–6100Å at 1-Å intervals, *Appl. Opt.* 13:518–522.

Trenberth, K. E. (1992), *Climate System Modeling*, Cambridge University Press, London, pp. 788.

Varotsos, C. A., and Cracknell, A. P. (1994), Three years of total ozone measurements over Athens obtained using the remote sensing technique of a Dobson spectrophotometer, *Int. J. Remote Sens.* 15:1519–1524.

WCP-112 (1986), *A Preliminary Cloudless Standard Atmosphere for Radiation Computation*, World Meteorological Organization, Geneva, Switzerland, 53 pp.